SCIENCE CHINA
Mathematics

• ARTICLES •

December 2017 Vol. 60 No. 12: 2515–2530
doi: 10.1007/s11425-016-9118-x

A conservative local discontinuous Galerkin method for the solution of nonlinear Schrödinger equation in two dimensions

ZHANG RongPei[1], YU XiJun[2], LI MingJun[3,*] & LI XiangGui[4]

[1]*School of Mathematics and Systematic Sciences, Shenyang Normal University, Shenyang* 110034*, China;*
[2]*Laboratory of Computational Physics, Institute of Applied Physics and Computational Mathematics, Beijing* 100088*, China;*
[3]*School of Mathematics and Computational Science, Xiangtan University, Xiangtan* 411105*, China;*
[4]*School of Applied Science, Beijing Information Science and Technology University, Beijing* 100192*, China*

*Email: rongpeizhang@*163*.com, yuxj@iapcm.ac.cn, alimingjun@*163*.com, lixg@bistu.edu.cn*

Received January 19, 2017; accepted June 15, 2017; published online September 25, 2017

Abstract In this study, we present a conservative local discontinuous Galerkin (LDG) method for numerically solving the two-dimensional nonlinear Schrödinger (NLS) equation. The NLS equation is rewritten as a first-order system and then we construct the LDG formulation with appropriate numerical flux. The mass and energy conserving laws for the semi-discrete formulation can be proved based on different choices of numerical fluxes such as the central, alternative and upwind-based flux. We will propose two kinds of time discretization methods for the semi-discrete formulation. One is based on Crank-Nicolson method and can be proved to preserve the discrete mass and energy conservation. The other one is Krylov implicit integration factor (IIF) method which demands much less computational effort. Various numerical experiments are presented to demonstrate the conservation law of mass and energy, the optimal rates of convergence, and the blow-up phenomenon.

Keywords discontinuous Galerkin method, nonlinear Schrödinger equation, conservation, Krylov implicit integration factor method

MSC(2010) 65M12, 65M60

Citation: Zhang R P, Yu X J, Li M J, et al. A conservative local discontinuous Galerkin method for the solution of nonlinear Schrödinger equation in two dimensions. Sci China Math, 2017, 60: 2515–2530, doi: 10.1007/s11425-016-9118-x

1 Introduction

In this paper, we consider the two-dimensional nonlinear Schrödinger (NLS) equation with cubic nonlinearity

$$\mathrm{i}u_t + \Delta u + |u|^2 u = 0, \quad (x, y) \in \mathbb{R}^2, \quad t \geqslant 0, \tag{1.1}$$

where u is a complex-valued function, $\mathrm{i} = \sqrt{-1}$ is the imaginary unit and Δ is the Laplace operator. The NLS equation plays an important role in many fields of physics (see [5,11,32]) as an initial-value problem with initial condition

$$u(x, y, 0) = u_0(x, y). \tag{1.2}$$

* Corresponding author

For example, in nonlinear optics, the NLS equation describes in certain regimes the propagation of electromagnetic beams in media whose index of refraction depends on the amplitude of the field in a simple nonlinear way (see [9]).

In this paper, we shall be interested in the numerical approximation of the blow-up solution of (1.1) with some radially symmetric initial value (1.2) in two dimensions. Since the initial-value problem (1.1) –(1.2) is defined over the entire plane, application of the numerical scheme requires the truncation of the whole plane into a bounded domain Ω. We set the boundary condition as the homogeneous Dirichlet boundary condition

$$u(x,y)=0, \quad (x,y)\in\partial\Omega. \tag{1.3}$$

It is easy to prove that the initial value problem (1.1)–(1.2) with homogeneous Dirichlet boundary condition (1.3) admits mass conservation law

$$Q(t)=\int_\Omega |u(x,y,t)|^2dxdy\equiv\int_\Omega |u_0|^2dxdy=Q(0) \tag{1.4}$$

and the energy conservation law

$$E(t)=\int_\Omega\left(|\nabla u(x,y,t)|^2-\frac{1}{2}|u(x,y,t)|^4\right)dxdy\equiv\int_\Omega\left(|\nabla u_0|^2-\frac{1}{2}|u_0|^4\right)dxdy=E(0) \tag{1.5}$$

for $t>0$.

It is well known that there are singular solutions of (1.1) for suitable initial condition data. Elaborate mathematical researches have been carried out on the blow-up properties of the solutions for the NLS equation. Merle and Tsutsumi [26] proved that, for a blow-up solution with a radially symmetric initial data, the origin is a blow-up point and an L^2-concentration phenomenon occurs at the origin. Furthermore, for arbitrary k points $(x_1,y_1),(x_2,y_2),\ldots,(x_k,y_k)$ in $\mathbb{R}^2$, Merle [25] constructed a blow-up solution which blows up exactly at these k points, and described its local behavior at $\{(x_1,y_1),(x_2,y_2),\ldots,(x_k,y_k)\}$. In this paper, we will study the numerical solution of NLS equation to have a better understanding of the blow-up solutions' behavior and in particular of the local behavior of these solutions.

There have been extensive studies on developing the numerical methods to compute the NLS equation. These methods include the spectral (pseudospectral) method (see [3,29]), finite difference method (FDM) (see [7,12,13,20,30,31,33,36]), finite element method (FEM) (see [1,14,17,18]) and collocation method (see [16,23,40]). For more numerical methods the reader may consult the reference [2]. Experience reveals that the mass and energy conserving numerical methods, which conserve the discrete approximation of the mass and energy, are favorable because they are able to maintain the phase and shape of the soliton waves accurately, especially for long time integration.

Recently, discontinuous Galerkin (DG) methods were popular in solving some nonlinear diffusion problems (see [21, 24, 39]). The application of DG methods possesses such advantages: they can handle complicated geometries and adaptivity well; they are robust and non-oscillatory in the presence of high gradients, even blow-up; they can maintain high order of accuracy; for time-dependent problems, they are especially well suited for the implicit integration factor time integration method because their mass matrices are block diagonal.

The DG methods' popularity has also attracted researchers to solve some Schrödinger equations by the DG discretization. Xu and Shu [34] developed the LDG method to solve the generalized NLS. In [37], Zhang et al. have applied the direct DG method to NLS and proved the mass conservation. Lu et al. [22] presented a mass preserving DG method for linear Schrödinger equation. All these methods can be proved to preserve the discrete mass conservation law; however, we do not find that there are any proofs about the discrete energy conservation law. Recently, Liang et al. [19] studied a mass preserving LDG method combined with the fourth order exponential time differencing Runge-Kutta method. Hong et al. [15] proposed a conservative LDG method with upwind-biased numerical fluxes. The two proceeding conservative LDG methods are confined to the one-dimensional NLS equation. In this paper, we apply the LDG method to solve the two-dimensional NLS equation and prove that this method can satisfy the

discrete mass and energy conserving laws. We rewrite the NLS equation as a first-order system and then apply the DG method on the system. The key ingredient for the success of the conservative LDG method is the correct design of interface numerical fluxes. In the design of the numerical fluxes, the role of the auxiliary parameters is to ensure the conservation and enhance the accuracy of the method. The first LDG method was proposed by Cockburn and Shu [10] for solving convection diffusion equation containing second derivatives. Thereafter, the LDG methods were widely applied to solve general nonlinear PDEs with the features of local conservation and stability. For the detailed description about the application of LDG methods, we refer the readers to the survey paper [35].

After the DG discretization of the NLS equation, we get a system of nonlinear complex ordinary differential equations (ODEs). The implicit time integration method is necessary because of nonlinear terms. We will propose two kinds of time discretization methods for the semi-discrete formulation. One is based on Crank-Nicolson method and can be proved to preserve the discrete mass and energy conservation. The other one is Krylov implicit integration factor (IIF) method which demands much less computational effort. The DG discretization leads to a relatively large number of degrees of freedom in comparison to other discretization methods, especially in high dimension case. If ones use implicit time integration method, the corresponding nonlinear systems are large and cause enormous computational cost. Thus, there is the need for suitable time discretization technique to improve the overall efficiency and performance of the DG method. In this paper, we will apply the Krylov implicit integration factor (IIF) method (see [8, 38]), which demands much less computational effort. This method treats the linear diffusions exactly and explicitly, and the nonlinear reactions implicitly. For the linear part, to efficiently evaluate the product of the matrix exponential and a vector, we perform Krylov subspace approximations. For the nonlinear part, we will solve the algebraic systems by Picard iteration or Newton iteration. A novel feature of this method is that the nonlinear algebraic systems can be solved element by element. So it preserves the "local" property of the DG method. Although there is no proof of mass and energy conservation for the IIF method, we can numerically observe that its mass and energy keep invariant in time.

The rest of the paper is organized as follows: In Section 2, we present the semi-discrete DG method combined with the appropriate numerical flux. We prove the mass and energy conservation laws in semi-discrete formulation. The fully discrete DG method combined with two kinds of time discretization method is presented in Section 3. Numerical experiments are reported in Section 4 to demonstrate the optimal convergence rates and mass and energy conservation of proposed DG method, as well as its excellent capability of capturing blow-up. Finally, we summarize our conclusion in Section 5.

2 Discontinuous Galerkin method

2.1 Notation

We consider a two-dimensional computation domain Ω which is discretized into triangular cells $\mathcal{T}_h = \{K\}$. We denote by $\mathcal{E}_h = \mathcal{E}_h^0 \cup \partial\Omega$ the set of all edges of $\mathcal{T}_h$, where $\mathcal{E}_h^0$ is the set of all interior edges. We define the DG approximation space as

$$\begin{aligned} V_h &= \{v \in L^2(\Omega) : v|_K \in P^k(K), \forall\, K \in \mathcal{T}_h\}, \\ \Sigma_h &= \{\boldsymbol{q} \in [L^2(\Omega)]^2 : \boldsymbol{q}|_K \in \Sigma(K), \forall\, K \in \mathcal{T}_h\}, \end{aligned} \tag{2.1}$$

where $P^k(K)$ is the space of complex polynomial functions of degree at most k on element K and $\Sigma(K) = [P^k(K)]^2$. The DG approximation space (2.1) is equipped with the following broken L^2 norm:

$$|||v|||^2 = \sum_{K\in\mathcal{T}_h} \|v\|^2_{L^2(K)}, \quad |||\boldsymbol{q}|||^2 = \sum_{K\in\mathcal{T}_h} \|\boldsymbol{q}_h\|^2_{L^2(K)}, \tag{2.2}$$

and broken L^4 norm

$$|||v|||_4^4 = \sum_{K\in\mathcal{T}_h} \|v\|^4_{L^4(K)}, \tag{2.3}$$

respectively.

We define the average and jump trace operators on edge e as follows. Let $e \in \mathcal{E}_h^0$ be an interior edge shared by element K_1 and K_2. We assume that the normal vectors $\boldsymbol{n_1}$ and $\boldsymbol{n_2}$ on e point exterior to K_1 and K_2, respectively. With two traces of function $v_i := v|_{\partial K_i}, i = 1, 2$, the average and jump of v along e are defined as

$$\{v\} = \frac{1}{2}(v_1 + v_2), \quad [\![v]\!] = v_1\boldsymbol{n_1} + v_2\boldsymbol{n_2}.$$

The average and jump for the vector function $\boldsymbol{q}$ can be analogously defined as follows:

$$\{\boldsymbol{q}\} = \frac{1}{2}(\boldsymbol{q_1} + \boldsymbol{q_2}), \quad [\![\boldsymbol{q}]\!] = \boldsymbol{q_1} \cdot \boldsymbol{n_1} + \boldsymbol{q_2} \cdot \boldsymbol{n_2}.$$

Notice that the jump $[\![v]\!]$ of the scalar function v is a vector parallel to the normal, and the jump $[\![\boldsymbol{q}]\!]$ of the vector function $\boldsymbol{q}$ is a scalar quantity.

We will discuss the homogeneous Dirichlet boundary condition (extension to other boundary condition is straightforward), i.e., that $u = 0$, on $\partial\Omega$. For this boundary condition, we only require the quantities $[\![v]\!]$ and $\{\boldsymbol{q}\}$ which are set as

$$[\![v]\!] = v\boldsymbol{n}, \quad \{\boldsymbol{q}\} = \boldsymbol{q},$$

where $\boldsymbol{n}$ is the outward unit normal.

2.2 The DG discretization

In this subsection, we only give the semi-discrete DG method for the NLS equation (1.1) and leave the time dependence continuous. The time integration method will be presented in Section 3. To obtain the energy conserving scheme, we need rewrite the NLS equation (1.1) into a first order system by introducing the auxiliary vector function $\boldsymbol{p}$:

$$\begin{aligned} &\boldsymbol{p} = \nabla u, \\ &\mathrm{i}u_t + \nabla \cdot \boldsymbol{p} + |u|^2 u = 0. \end{aligned} \tag{2.4}$$

Following [34], the general DG formulation for (2.4) is to find $u_h \in V_h$ and $\boldsymbol{p_h} \in \Sigma_h$ such that

$$\begin{aligned} &\int_K \boldsymbol{p_h} \cdot \boldsymbol{q} dxdy + \int_K u_h \nabla \cdot \boldsymbol{q} dxdy - \int_{\partial K} \widehat{u_h}\boldsymbol{q} \cdot \boldsymbol{n} ds = 0, \\ &\mathrm{i}\int_K (u_h)_t v dxdy - \int_K \boldsymbol{p_h} \cdot \nabla v dxdy + \int_{\partial K} \widehat{\boldsymbol{p_h}} \cdot \boldsymbol{n} v ds + \int_K |u_h|^2 u_h v dxdy = 0, \end{aligned} \tag{2.5}$$

for all $K \in \mathcal{T}_h$. Here, $\widehat{u_h}$ and $\widehat{\boldsymbol{p_h}}$ are numerical fluxes which are single values on the edge of element K as the approximation of u and $\boldsymbol{p} = \nabla u$, respectively. These fluxes have to be suitably defined in order to ensure the conservation of the method and enhance its accuracy.

With this choice of these numerical flux, we add (2.5) over all the elements to obtain the following LDG scheme:

$$\int_\Omega \boldsymbol{p_h} \cdot \boldsymbol{q} dxdy + \sum_{K \in \mathcal{T}_h} \int_K u_h \nabla \cdot \boldsymbol{q} dxdy - \int_{\mathcal{E}_h^0} \widehat{u_h} [\![\boldsymbol{q}]\!] ds = 0, \tag{2.6}$$

$$\mathrm{i}\int_\Omega (u_h)_t v dxdy - \sum_{K \in \mathcal{T}_h} \int_K \boldsymbol{p_h} \cdot \nabla v dxdy + \int_{\mathcal{E}_h} \widehat{\boldsymbol{p_h}} \cdot [\![v]\!] ds + \int_\Omega |u_h|^2 u_h v dxdy = 0, \tag{2.7}$$

for all test functions $v \in V_h$ and $\boldsymbol{q} \in \Sigma_h$.

We are now ready to define the numerical fluxes in (2.6)–(2.7). If the edge e is inside the domain Ω, the LDG numerical fluxes are taken as [6, 27], i.e.,

$$\begin{aligned} &\widehat{u_h} = \{u_h\} + \boldsymbol{C_{12}} \cdot [\![u_h]\!], \\ &\widehat{\boldsymbol{p_h}} = \{\boldsymbol{p_h}\} - C_{11}[\![u_h]\!] - \boldsymbol{C_{12}}[\![\boldsymbol{p_h}]\!]. \end{aligned} \tag{2.8}$$

With the homogeneous Dirichlet boundary condition, the fluxes on the boundary are defined as

$$\begin{aligned} &\widehat{u_h} = 0, \\ &\widehat{\boldsymbol{p_h}} = \boldsymbol{p_h} - C_{11} u_h \boldsymbol{n}, \end{aligned} \tag{2.9}$$

where $\boldsymbol{n}$ is the outward unit normal. The auxiliary parameters $\boldsymbol{C_{12}}$ and C_{11} are independent of u_h and $\boldsymbol{p_h}$. Its role is to ensure the conservation and enhance the accuracy of the method. When the stabilization parameter C_{11} is of order h^{-1}, our numerical experiments in Section 4 give the optimal orders of convergence on structured triangulations. If the coefficient $C_{11} = 0$, we can prove that the LDG method (2.6)–(2.7) preserves the mass and energy conservation in Section 2. There are three numerical fluxes in the case of $C_{11} = 0$. When $\boldsymbol{C_{12}} = 0$ the flux (2.8) is central flux proposed by Bassi and Rebay [4]. When $\boldsymbol{C_{12}} = \frac{1}{2}\boldsymbol{n_1}$ or $\boldsymbol{C_{12}} = \frac{1}{2}\boldsymbol{n_2}$, the flux (2.8) is alternative flux which can result in narrow band in the LDG matrix formulation. We can extend the central and alternative flux into the general case, i.e., that $\boldsymbol{C_{12}} = \frac{1}{2}(\theta\boldsymbol{n_1} + (1-\theta)\boldsymbol{n_2})$, $0 \leqslant \theta \leqslant 1$, and this flux is called as upwind-biased flux which has been proposed in one-dimensional case in [15].

2.3 Conservation

In the design of the numerical schemes for the NLS equation, the discrete mass and energy conservation laws are generally taken into consideration. The schemes preserving the mass and energy conservation appear to approximate the solution better, especially in the long time behavior. In this subsection, we will prove that the semi-discrete DG method can conserve the mass and energy.

With the definition of broken L^2 norm (2.2) and L^4 norm (2.3), we define the discrete formulation of mass and energy as $Q_h(t) = |||u_h|||^2$, and $E_h(t) = |||\boldsymbol{p_h}|||^2 - \frac{1}{2}|||u_h|||_4^4$, respectively. Before we prove the conservation of scheme (2.6)–(2.7), we list a useful lemma as follows:

Lemma 2.1. *When the coefficient $C_{11} = 0$ in the numerical flux* (2.8) *and* (2.9)*, we have the following equality*:

$$\sum_{K\in\mathcal{T}_h}\int_K \boldsymbol{q}\cdot\nabla v dxdy + \sum_{K\in\mathcal{T}_h}\int_K v\nabla\cdot\boldsymbol{q} dxdy = \int_{\mathcal{E}_h^0}\widehat{v}[\![\boldsymbol{q}]\!]ds + \int_{\mathcal{E}_h}\widehat{\boldsymbol{q}}\cdot[\![v]\!]ds \tag{2.10}$$

for all $v \in V_h \cap H_0^1$ and $\boldsymbol{q} \in \Sigma_h$.

Proof. Applying the integration by part to the left-hand side, we have

$$\sum_{K\in\mathcal{T}_h}\int_K \boldsymbol{q}\cdot\nabla v dxdy + \sum_{K\in\mathcal{T}_h}\int_K v\nabla\cdot\boldsymbol{q} dxdy = \sum_{K\in\mathcal{T}_h}\int_{\partial K} v\boldsymbol{q}\cdot\boldsymbol{n} ds. \tag{2.11}$$

We use the average and jump operators to rewrite the sums of the element form into the edge form. A straightforward computation shows that

$$\sum_{K\in\mathcal{T}_h}\int_{\partial K} v\boldsymbol{q}\cdot\boldsymbol{n} dxdy = \int_{\mathcal{E}_h^0}\{v\}[\![\boldsymbol{q}]\!]ds + \int_{\mathcal{E}_h}\{\boldsymbol{q}\}\cdot[\![v]\!]ds. \tag{2.12}$$

Substituting the numerical flux (2.8) and (2.9) into the right-hand side to get

$$\begin{aligned} &\int_{\mathcal{E}_h^0}\widehat{v}[\![\boldsymbol{q}]\!]ds + \int_{\mathcal{E}_h}\widehat{\boldsymbol{q}}\cdot[\![v]\!]ds \\ &= \int_{\mathcal{E}_h^0}\{v\}[\![\boldsymbol{q}]\!]ds + \int_{\mathcal{E}_h}\{\boldsymbol{q}\}\cdot[\![v]\!]ds + \int_{\mathcal{E}_h^0}(\boldsymbol{C_{12}}\cdot[\![v]\!][\![\boldsymbol{q}]\!] - \boldsymbol{C_{12}}\cdot[\![v]\!][\![\boldsymbol{q}]\!])ds - C_{11}\int_{\mathcal{E}_h}[\![u]\!]\cdot[\![v]\!]ds \\ &= \int_{\mathcal{E}_h^0}\{v\}[\![\boldsymbol{q}]\!]ds + \int_{\mathcal{E}_h}\{\boldsymbol{q}\}\cdot[\![v]\!]ds - C_{11}\int_{\mathcal{E}_h}[\![u]\!]\cdot[\![v]\!]ds. \end{aligned}$$

With $C_{11} = 0$ we complete the proof. □

With Lemma 2.1, we have the following mass and energy conservation for the semi-discrete LDG scheme (2.6)–(2.7).

Theorem 2.2. *With the homogeneous Dirichlet boundary condition and the coefficient* $C_{11}=0$ *in the numerical flux* (2.8) *and* (2.9)*, the scheme* (2.6)–(2.7) *preserves the mass conservation law in semi-discrete formulation*

$$\frac{d}{dt}Q_h(t)\equiv 0. \tag{2.13}$$

Proof. In (2.6), we choose the test function $\boldsymbol{q}=\boldsymbol{p}_{\boldsymbol{h}}^*$ where the superscript * denotes the complex conjugate. We can obtain

$$|||\boldsymbol{p}_{\boldsymbol{h}}|||^2+\sum_{K\in\mathcal{T}_h}\int_K u_h\nabla\cdot\boldsymbol{p}_{\boldsymbol{h}}^* dxdy-\int_{\mathcal{E}_h^0}\widehat{u_h}[\![\boldsymbol{p}_{\boldsymbol{h}}^*]\!]ds=0. \tag{2.14}$$

Taking the complex conjugate for every term in (2.14), we get

$$|||\boldsymbol{p}_{\boldsymbol{h}}|||^2+\sum_{K\in\mathcal{T}_h}\int_K u_h^*\nabla\cdot\boldsymbol{p}_{\boldsymbol{h}} dxdy-\int_{\mathcal{E}_h^0}\widehat{u_h}^*[\![\boldsymbol{p}_{\boldsymbol{h}}]\!]ds=0. \tag{2.15}$$

We take the difference between (2.14) and (2.15) to get

$$\sum_{K\in\mathcal{T}_h}\int_K 2\mathrm{Im}(u_h^*\nabla\cdot\boldsymbol{p}_{\boldsymbol{h}})dxdy-\int_{\mathcal{E}_h^0}2\mathrm{Im}(\widehat{u_h}^*[\![\boldsymbol{p}_{\boldsymbol{h}}]\!])ds=0, \tag{2.16}$$

where $\mathrm{Im}(u)$ means the imaginary part and $\mathrm{Re}(u)$ the real part of a complex function u.

Now we take $v=u_h^*$ in (2.7) to obtain

$$\mathrm{i}\int_\Omega(u_h)_t u_h^* dxdy-\sum_{K\in\mathcal{T}_h}\int_K\boldsymbol{p}_{\boldsymbol{h}}\cdot\nabla u_h^* dxdy+\int_{\mathcal{E}_h}\widehat{\boldsymbol{p}_{\boldsymbol{h}}}\cdot[\![u_h^*]\!]ds+|||u_h|||_4^4=0. \tag{2.17}$$

Similarly, we take the complex conjugate for every term in (2.17),

$$-\mathrm{i}\int_\Omega(u_h)_t^* u_h dxdy-\sum_{K\in\mathcal{T}_h}\int_K\boldsymbol{p}_{\boldsymbol{h}}^*\cdot\nabla u_h dxdy+\int_{\mathcal{E}_h}\widehat{\boldsymbol{p}_{\boldsymbol{h}}}^*\cdot[\![u_h]\!]ds+|||u_h|||_4^4=0, \tag{2.18}$$

then take the difference between (2.17) and (2.18) and multiply imaginary unit "i" on the both sides to obtain

$$\frac{d}{dt}|||u_h|||^2-\sum_{K\in\mathcal{T}_h}\int_K 2\mathrm{Im}(\boldsymbol{p}_{\boldsymbol{h}}\cdot\nabla u_h^*)dxdy+\int_{\mathcal{E}_h}2\mathrm{Im}(\widehat{\boldsymbol{p}_{\boldsymbol{h}}}\cdot[\![u_h^*]\!])ds=0. \tag{2.19}$$

Taking $C_{11}=0$ in (2.10) and subtracting (2.19) from (2.16), we can get $\frac{d}{dt}|||u_h|||^2=0$ which gives (2.13). □

Theorem 2.3. *Take the coefficient* $C_{11}=0$ *in the numerical flux* (2.8) *and* (2.9)*, the DG scheme* (2.6)–(2.7) *can preserve the semi-discrete energy conservation law*

$$\frac{d}{dt}E_h(t)\equiv 0. \tag{2.20}$$

Proof. By taking the time derivative of (2.6) and choosing the test function $\boldsymbol{q}=\boldsymbol{p}_{\boldsymbol{h}}^*$, we obtain

$$\sum_{K\in\mathcal{T}_h}\int_K(\boldsymbol{p}_{\boldsymbol{h}})_t\cdot\boldsymbol{p}_{\boldsymbol{h}}^* dxdy+\sum_{K\in\mathcal{T}_h}\int_K(u_h)_t\nabla\cdot\boldsymbol{p}_{\boldsymbol{h}}^* dxdy-\int_{\mathcal{E}_h^0}(\widehat{u_h})_t[\![\boldsymbol{p}_{\boldsymbol{h}}^*]\!]ds=0. \tag{2.21}$$

Taking the complex conjugate for (2.21), we have

$$\sum_{K\in\mathcal{T}_h}\int_K(\boldsymbol{p}_{\boldsymbol{h}}^*)_t\cdot\boldsymbol{p}_{\boldsymbol{h}} dxdy+\sum_{K\in\mathcal{T}_h}\int_K(u_h^*)_t\nabla\cdot\boldsymbol{p}_{\boldsymbol{h}} dxdy-\int_{\mathcal{E}_h^0}(\widehat{u_h}^*)_t[\![\boldsymbol{p}_{\boldsymbol{h}}]\!]ds=0. \tag{2.22}$$

Summing up (2.21) and (2.22), we have

$$\frac{d}{dt}|||\boldsymbol{p}_{\boldsymbol{h}}|||^2+\sum_{K\in\mathcal{T}_h}\int_K 2\mathrm{Re}((u_h)_t\nabla\cdot\boldsymbol{p}_{\boldsymbol{h}}^*)dxdy-\int_{\mathcal{E}_h^0}2\mathrm{Re}((\widehat{u_h})_t[\![\boldsymbol{p}_{\boldsymbol{h}}^*]\!])ds=0. \tag{2.23}$$

In (2.7), we choose the test function $v = (u_h^*)_t$ and get

$$\mathrm{i}|||(u_h)_t|||^2 - \sum_{K\in\mathcal{T}_h}\int_K \boldsymbol{p_h}\cdot\nabla(u_h^*)_t dxdy + \int_{\mathcal{E}_h}\widehat{\boldsymbol{p_h}}\cdot[\![(u_h^*)_t]\!]ds + \sum_{K\in\mathcal{T}_h}\int_K |u_h|^2 u_h(u_h^*)_t dxdy = 0. \quad (2.24)$$

We also take the complex conjugate for (2.24) to obtain

$$-\mathrm{i}|||(u_h)_t|||^2 - \sum_{K\in\mathcal{T}_h}\int_K \boldsymbol{p_h}^*\cdot\nabla(u_h)_t dxdy + \int_{\mathcal{E}_h}\widehat{\boldsymbol{p_h}}^*\cdot[\![(u_h)_t]\!]ds + \sum_{K\in\mathcal{T}_h}\int_K |u_h|^2 u_h^*(u_h)_t dxdy = 0. \quad (2.25)$$

Summing up (2.24) and (2.25), we have

$$-\sum_{K\in\mathcal{T}_h}\int_K 2\mathrm{Re}(\boldsymbol{p_h}\cdot\nabla(u_h^*)_t)dxdy + \int_{\mathcal{E}_h}2\mathrm{Re}(\widehat{\boldsymbol{p_h}}\cdot[\![(u_h^*)_t]\!])ds + \frac{1}{2}\frac{d}{dt}|||u_h|||_4^4 = 0. \quad (2.26)$$

Taking the difference of (2.23) and (2.26), together with the real part of (2.10) in which $v = (u_h^*)_t$ and $\boldsymbol{q} = \boldsymbol{p_h}$, we can get $\frac{d}{dt}|||\boldsymbol{p_h}|||^2 - \frac{1}{2}\frac{d}{dt}|||u_h|||_4^4 = 0$ which completes the proof. □

3 Time discretization

In the preceding section, we have proved that the semi-discrete LDG scheme (2.6)–(2.7) with numerical flux (2.8)–(2.9) preserves mass and energy conservation when $C_{11} = 0$. In order to extend the mass and energy conservation property to the fully discrete method, it is natural to employ time discretization methods which also conserve discrete mass and energy. In this section, we will consider two kinds of time discretization methods for the semi-discrete formulation. One is based on Crank-Nicolson method and can be proved to preserve the discrete mass and energy conservation. The other one is Krylov implicit integration factor (IIF) method which demands much less computational effort and can be numerically observed to preserve the mass and energy conservation.

3.1 Conservative time discretization method

For the semi-discrete LDG scheme (2.6)–(2.7), we construct the time discretization method as follows:

$$\int_\Omega \boldsymbol{p}_h^{n+1}\cdot\boldsymbol{q}dxdy + \sum_{K\in\mathcal{T}_h}\int_K u_h^{n+1}\nabla\cdot\boldsymbol{q}dxdy - \int_{\mathcal{E}_h^0}\widehat{u_h}^{n+1}[\![\boldsymbol{q}]\!]ds = 0, \quad (3.1)$$

$$\int_\Omega \boldsymbol{p}_h^{n}\cdot\boldsymbol{q}dxdy + \sum_{K\in\mathcal{T}_h}\int_K u_h^{n}\nabla\cdot\boldsymbol{q}dxdy - \int_{\mathcal{E}_h^0}\widehat{u_h}^{n}[\![\boldsymbol{q}]\!]ds = 0, \quad (3.2)$$

$$\mathrm{i}\int_\Omega \frac{u_h^{n+1}-u_h^n}{\Delta t}vdxdy - \sum_{K\in\mathcal{T}_h}\int_K \frac{\boldsymbol{p}_h^n+\boldsymbol{p}_h^{n+1}}{2}\cdot\nabla v dxdy + \int_{\mathcal{E}_h}\frac{\widehat{\boldsymbol{p_h}}^{n+1}+\widehat{\boldsymbol{p_h}}^{n}}{2}\cdot[\![v]\!]ds$$
$$+\int_\Omega \frac{|u_h^{n+1}|^2+|u_h^n|^2}{2}\frac{u_h^{n+1}+u_h^n}{2}vdxdy = 0, \quad (3.3)$$

for all test functions $v \in V_h$ and $\boldsymbol{q} \in \Sigma_h$.

Similar to Theorems 2.2 and 2.3, we have the following mass and energy conservation for the fully discrete LDG scheme (3.1)–(3.3).

Theorem 3.1. *Take $C_{11} = 0$ in the numerical flux* (2.8) *and* (2.9)*. The scheme* (3.1)–(3.3) *preserves the mass conservation law in fully discrete formulation*

$$|||u_h^{n+1}|||^2 = |||u_h^n|||^2 = \cdots = |||u_h^0|||^2. \quad (3.4)$$

Proof. In (3.1) and (3.2), we choose the test function $\boldsymbol{q} = \frac{(\boldsymbol{p_h^n}+\boldsymbol{p_h^{n+1}})^*}{2}$ and take the sum between them. We can obtain

$$\left|\left|\left|\frac{(\boldsymbol{p_h^n}+\boldsymbol{p_h^{n+1}})^*}{2}\right|\right|\right|^2 + \sum_{K\in\mathcal{T}_h}\int_K (u_h^{n+1}+u_h^n)\nabla\cdot\frac{(\boldsymbol{p_h^n}+\boldsymbol{p_h^{n+1}})^*}{2}dxdy$$

$$-\int_{\mathcal{E}_h^0}(\widehat{u_h}^n+\widehat{u_h}^{n+1})\left[\!\!\left[\frac{\boldsymbol{p_h^n}+\boldsymbol{p_h^{n+1}}}{2}\right]\!\!\right]^* ds=0. \tag{3.5}$$

Taking the imaginary part in (3.5), we get

$$\sum_{K\in\mathcal{T}_h}\int_K \mathrm{Im}\bigg((u_h^n+u_h^{n+1})^*\nabla\cdot\frac{\boldsymbol{p_h^n}+\boldsymbol{p_h^{n+1}}}{2}\bigg)dxdy$$
$$-\int_{\mathcal{E}_h^0}\mathrm{Im}\bigg((\widehat{u_h}^n+\widehat{u_h}^{n+1})^*\left[\!\!\left[\frac{\boldsymbol{p_h^n}+\boldsymbol{p_h^{n+1}}}{2}\right]\!\!\right]\bigg)ds=0. \tag{3.6}$$

Then we take $v=(u_h^{n+1}+u_h^n)^*$ in (3.3) to obtain

$$\mathrm{i}\int_\Omega\frac{u_h^{n+1}-u_h^n}{\Delta t}(u_h^{n+1}+u_h^n)^*dxdy-\sum_{K\in\mathcal{T}_h}\int_K\frac{\boldsymbol{p_h^n}+\boldsymbol{p_h^{n+1}}}{2}\cdot\nabla(u_h^{n+1}+u_h^n)^*dxdy$$
$$+\int_{\mathcal{E}_h}\frac{\widehat{\boldsymbol{p_h}}^{\boldsymbol{n+1}}+\widehat{\boldsymbol{p_h}}^{\boldsymbol{n}}}{2}\cdot[\![u_h^{n+1}+u_h^n]\!]^*ds+\int_\Omega\frac{|u_h^{n+1}|^2+|u_h^n|^2}{2}\frac{|u_h^{n+1}+u_h^n|^2}{2}dxdy=0. \tag{3.7}$$

Similarly, we take the imaginary part in (3.7) to get

$$\frac{|||u_h^{n+1}|||^2-|||u_h^n|||^2}{\Delta t}-\sum_{K\in\mathcal{T}_h}\int_K\mathrm{Im}\bigg(\frac{\boldsymbol{p_h^n}+\boldsymbol{p_h^{n+1}}}{2}\cdot\nabla(u_h^{n+1}+u_h^n)^*\bigg)dxdy$$
$$+\int_{\mathcal{E}_h}\mathrm{Im}\bigg(\frac{\widehat{\boldsymbol{p_h}}^{\boldsymbol{n+1}}+\widehat{\boldsymbol{p_h}}^{\boldsymbol{n}}}{2}\cdot[\![u_h^{n+1}+u_h^n]\!]^*\bigg)ds=0. \tag{3.8}$$

When $C_{11}=0$, the flux operator (2.8) is linear, we have $\widehat{u_h}^{n+1}+\widehat{u_h}^n=\widehat{u_h^{n+1}+u_h^n}$ and $\widehat{\boldsymbol{p_h}}^{\boldsymbol{n+1}}+\widehat{\boldsymbol{p_h}}^{\boldsymbol{n}}=\widehat{\boldsymbol{p_h}^{\boldsymbol{n+1}}+\boldsymbol{p_h^n}}$. Taking the difference of (3.6) and (3.8), we can get $|||u_h^{n+1}|||^2=|||u_h^n|||^2$ by using Lemma 2.1 with $v=(u_h^{n+1}+u_h^n)^*$ and $\boldsymbol{q}=\frac{\boldsymbol{p_h^n}+\boldsymbol{p_h^{n+1}}}{2}$. Carrying on like this we can complete the proof. □

Theorem 3.2. *With $C_{11}=0$ in the numerical flux* (2.8) *and* (2.9)*, the scheme* (3.1)–(3.3) *preserves the following energy conservation law in fully discrete formulation*:

$$|||\boldsymbol{p_h^{n+1}}|||^2-\frac{1}{2}|||u_h^{n+1}|||_4^4=|||\boldsymbol{p_h^n}|||^2-\frac{1}{2}|||u_h^n|||_4^4=\cdots=|||\boldsymbol{p_h^0}|||^2-\frac{1}{2}|||u_h^0|||_4^4. \tag{3.9}$$

Proof. In (3.1) and (3.2), we choose the test function $\boldsymbol{q}=\frac{(\boldsymbol{p_h^n}+\boldsymbol{p_h^{n+1}})^*}{2}$ and take the difference between them to obtain

$$\int_\Omega(\boldsymbol{p_h^{n+1}}-\boldsymbol{p_h^n})\cdot\frac{(\boldsymbol{p_h^n}+\boldsymbol{p_h^{n+1}})^*}{2}dxdy+\sum_{K\in\mathcal{T}_h}\int_K(u_h^{n+1}-u_h^n)\nabla\cdot\frac{(\boldsymbol{p_h^n}+\boldsymbol{p_h^{n+1}})^*}{2}dxdy$$
$$-\int_{\mathcal{E}_h^0}(\widehat{u_h}^{n+1}-\widehat{u_h}^n)\left[\!\!\left[\frac{\boldsymbol{p_h^n}+\boldsymbol{p_h^{n+1}}}{2}\right]\!\!\right]^*ds=0. \tag{3.10}$$

Taking the real part in (3.10), we get

$$\frac{|||\boldsymbol{p_h^{n+1}}|||^2-|||\boldsymbol{p_h^n}|||^2}{2}+\sum_{K\in\mathcal{T}_h}\int_K\mathrm{Re}\bigg((u_h^{n+1}-u_h^n)^*\nabla\cdot\frac{\boldsymbol{p_h^n}+\boldsymbol{p_h^{n+1}}}{2}\bigg)dxdy$$
$$-\int_{\mathcal{E}_h^0}\mathrm{Re}\bigg((\widehat{u_h}^{n+1}-\widehat{u_h}^n)^*\left[\!\!\left[\frac{\boldsymbol{p_h^n}+\boldsymbol{p_h^{n+1}}}{2}\right]\!\!\right]\bigg)ds=0. \tag{3.11}$$

Then we take $v=(u_h^{n+1}-u_h^n)^*$ in (3.3) to obtain

$$\frac{\mathrm{i}}{\Delta t}|||u_h^{n+1}-u_h^n|||^2-\sum_{K\in\mathcal{T}_h}\int_K\frac{\boldsymbol{p_h^n}+\boldsymbol{p_h^{n+1}}}{2}\cdot\nabla(u_h^{n+1}-u_h^n)^*dxdy$$

$$+\int_{\mathcal{E}_h}\frac{\widehat{\boldsymbol{p_h}}^{\boldsymbol{n+1}}+\widehat{\boldsymbol{p_h}}^{\boldsymbol{n}}}{2}\cdot[\![u_h^{n+1}-u_h^n]\!]^*ds+\int_\Omega\frac{|u_h^{n+1}|^2+|u_h^n|^2}{2}\frac{u_h^{n+1}+u_h^n}{2}(u_h^{n+1}-u_h^n)^*dxdy=0. \quad (3.12)$$

Now we take the real part of (3.12) to get

$$\begin{aligned}&-\sum_{K\in\mathcal{T}_h}\int_K\mathrm{Re}\bigg(\frac{\boldsymbol{p_h^n}+\boldsymbol{p_h^{n+1}}}{2}\cdot\nabla(u_h^{n+1}-u_h^n)^*\bigg)dxdy\\&+\int_{\mathcal{E}_h}\mathrm{Re}\bigg(\frac{\widehat{\boldsymbol{p_h}}^{\boldsymbol{n+1}}+\widehat{\boldsymbol{p_h}}^{\boldsymbol{n}}}{2}\cdot[\![u_h^{n+1}-u_h^n]\!]^*\bigg)ds+\frac{|||u_h^{n+1}|||_4^4-|||u_h^n|||_4^4}{4}=0.\end{aligned} \quad (3.13)$$

Taking the difference of (3.11) and (3.13) and using Lemma 2.1 with $v=(u_h^{n+1}-u_h^n)^*$ and $\boldsymbol{q}=\frac{\boldsymbol{p_h^n}+\boldsymbol{p_h^{n+1}}}{2}$, we have $|||\boldsymbol{p_h^{n+1}}|||^2-\frac{1}{2}|||u_h^{n+1}|||_4^4=|||\boldsymbol{p_h^n}|||^2-\frac{1}{2}|||u_h^n|||_4^4$. Carrying on like this we can complete the proof. □

3.2 Krylov implicit integration factor method

Although the time-discretization scheme (3.1)–(3.3) is conservative, there are some difficulties in solving the nonlinear complex systems. As a main drawback, the LDG method has relatively large number of degrees of freedom compared with other methods. Moreover, the solution of large nonlinear complex algebraic systems causes enormous computational cost. We will use the Krylov IIF method which demands much less computational effort. To apply the Krylov IIF method, we first write the LDG scheme (2.6)–(2.7) into the matrix equation of the form

$$\boldsymbol{M_1P}=\boldsymbol{A_1U}, \quad (3.14)$$

$$\mathrm{i}\boldsymbol{M_2}\frac{d\boldsymbol{U}}{dt}=\boldsymbol{A_2P}+\boldsymbol{F_N}(\boldsymbol{U}), \quad (3.15)$$

where $\boldsymbol{U}$ and $\boldsymbol{P}$ are solution vectors containing the degrees of freedom of u and $\boldsymbol{p}$ and $\boldsymbol{F_N}(\boldsymbol{U})$ is from the nonlinear term $|u|^2u$. Since the mass matrices $\boldsymbol{M_1}$ and $\boldsymbol{M_2}$ are block diagonal, we can invert them easily. Solving $\boldsymbol{P}$ from (3.14), $\boldsymbol{P}=\boldsymbol{M_1^{-1}A_1U}$, and substituting it into (3.15), we obtain the following nonlinear complex ODE system:

$$\frac{d\boldsymbol{U}}{dt}=\boldsymbol{AU}+\boldsymbol{F}(\boldsymbol{U}), \quad (3.16)$$

where $\boldsymbol{A}=-\mathrm{i}\boldsymbol{M_2^{-1}A_2}(\boldsymbol{M_1^{-1}A_1})$ and $\boldsymbol{F}(\boldsymbol{U})=-\mathrm{i}\boldsymbol{M_2^{-1}F_N}(\boldsymbol{U})$.

Assume the final time is $t=T$ and let time step $\Delta t=T/N$, $t_n=n\Delta t$, $0\leqslant n\leqslant N$. Following Chen and Zhang [8], we multiply (3.16) by the integration factor $\mathrm{e}^{-\boldsymbol{A}t}$ and integrate over one time step from t_n to t_{n+1} to obtain

$$\boldsymbol{U_{n+1}}=\mathrm{e}^{\boldsymbol{A}\Delta t}\boldsymbol{U_n}+\mathrm{e}^{\boldsymbol{A}\Delta t}\int_0^{\Delta t}\mathrm{e}^{-\boldsymbol{A}\tau}\boldsymbol{F}(\boldsymbol{U}(t_n+\tau))d\tau. \quad (3.17)$$

Approximating the integrand in (3.17) by using an $(r-1)$-th order Lagrange interpolation polynomial with interpolation points at $t_{n+1},t_n,\ldots,t_{n-r+2}$, we obtain the r-th IIF scheme

$$\boldsymbol{U_{n+1}}=\mathrm{e}^{\boldsymbol{A}\Delta t}\boldsymbol{U_n}+\Delta t\bigg(\alpha_1\boldsymbol{F}(\boldsymbol{U_{n+1}})+\sum_{j=0}^{r-2}\alpha_{-j}\mathrm{e}^{(j+1)\boldsymbol{A}\Delta t}\boldsymbol{F}(\boldsymbol{U}_{n-j})\bigg). \quad (3.18)$$

The values of coefficients α_j, $j=1,0,\ldots,2-r$ can be referred in [28]. The usual schemes include the second-order scheme (IIF2)

$$\boldsymbol{U_{n+1}}=\mathrm{e}^{\boldsymbol{A}\Delta t}\bigg(\boldsymbol{U_n}+\frac{\Delta t}{2}\boldsymbol{F}(\boldsymbol{U_n})\bigg)+\frac{\Delta t}{2}\boldsymbol{F}(\boldsymbol{U_{n+1}}) \quad (3.19)$$

and the third-order scheme (IIF3)

$$\boldsymbol{U_{n+1}}=\mathrm{e}^{\boldsymbol{A}\Delta t}\boldsymbol{U_n}+\Delta t\bigg(\frac{5}{12}\boldsymbol{F}(\boldsymbol{U_{n+1}})+\frac{2}{3}\mathrm{e}^{\boldsymbol{A}\Delta t}\boldsymbol{F}(\boldsymbol{U_n})-\frac{1}{12}\mathrm{e}^{2\boldsymbol{A}\Delta t}\boldsymbol{F}(\boldsymbol{U}_{n-1})\bigg). \quad (3.20)$$

In the computation, to be consistent with the order of accuracy in the spatial direction, we combine the P^1 DG discretization with IIF2 and P^2 DG spatial discretization with IIF3.

To solve the global nonlinear systems (3.17), we first compute the product of matrix exponential and a vector, for example $\mathrm{e}^{\boldsymbol{A}\Delta t}\boldsymbol{w}$. Although the discretization matrix A is sparse, their exponentials matrix will be dense. So we use Krylov subspace method to approximate the products of the exponential matrix and vector. The Krylov subspace method has been presented in [8]. But to make the paper self-contained, we will briefly describe it. The underlying principle is to project the large sparse matrix A to the Krylov subspace

$$\boldsymbol{K_m} = \mathrm{span}\{\boldsymbol{w}, A\boldsymbol{w}, \ldots, (A)^{m-1}\boldsymbol{w}\},$$

where m is the dimension of the Krylov subspace and is much smaller than the dimension of the large sparse matrix A. We take $m = 25$ in all numerical computations of this paper, and accurate results are obtained as shown in Section 4. Then we apply the Arnoldi algorithm to generate an orthonormal basis $\boldsymbol{V_{m+1}} = (\boldsymbol{v_1}, \ldots, \boldsymbol{v_{m+1}})$ and an $(m+1)\times(m+1)$ upper Hessenberg matrix $\overline{\boldsymbol{H}}_{\boldsymbol{m+1}} = [h_{ij}]$. The very small Hessenberg matrix $\overline{\boldsymbol{H}}_{\boldsymbol{m+1}}$ represents the projection of the large sparse matrix A to the Krylov subspace $\boldsymbol{K_m}$, with respect to the basis $\boldsymbol{V_{m+1}}$. Since the columns of $\boldsymbol{V_{m+1}}$ are orthonormal we get the approximation

$$\mathrm{e}^{A\Delta t}\boldsymbol{U_n} = \beta \boldsymbol{V_{m+1}} \mathrm{e}^{\Delta t \overline{\boldsymbol{H}}_{\boldsymbol{m+1}}} \boldsymbol{e_1}, \tag{3.21}$$

where $\boldsymbol{e_1}$ is the first unit basis vector, $\beta = \|\boldsymbol{w}\|_2$. The small matrix exponential $\mathrm{e}^{\Delta t \overline{\boldsymbol{H}}_{\boldsymbol{m+1}}}$ can be computed with a Padé approximation with only computational cost of $O((m+1)^2)$. Thus the large matrix exponential problem is replaced by a much smaller approximation.

Applying the Krylov subspace approximation to (3.18), we get nonlinear algebraic system

$$\boldsymbol{U_{n+1}} - \alpha_1 \Delta t \boldsymbol{F}(\boldsymbol{U_{n+1}}) - \boldsymbol{Q_n} = 0, \tag{3.22}$$

where $\boldsymbol{Q_n} = \mathrm{e}^{\boldsymbol{A}\Delta t}\boldsymbol{U_n} + \Delta t \sum_{j=0}^{r-2} \alpha_{-j} \mathrm{e}^{(j+1)\boldsymbol{A}\Delta t} \boldsymbol{F}(\boldsymbol{U_{n-j}})$ can be computed by (3.21). Notice that the nonlinear implicit term $\boldsymbol{F}(\boldsymbol{U_{n+1}})$ does not involve the matrix exponential operator. Hence the computation of it does not involve the coupling of the numerical values at the spatial grid points. So we can solve the nonlinear systems (3.22) locally by the classic nonlinear solver such as Newton or Picard iteration method.

4 Numerical experiments

In this section, we will demonstrate the performance of the proposed DG scheme on a number of test problems. Firstly, we test our scheme using the NLS equation which has the exact solution. In this test, we will show the optimal convergence rate, unconditional stability and robustness of the DG method numerically. Then we apply the DG scheme to approximate the blow-up solution of cubic NLS equation on a disk.

Example 4.1. Consider the following NLS equation on a rectangle $\Omega = [0, \pi]^2$:

$$\mathrm{i}u_t + \Delta u + |u|^2 u - \sin^2 x \sin^2 y u = 0, \quad t \geqslant 0 \tag{4.1}$$

with homogeneous Dirichlet boundary condition. The equation has the following exact solution:

$$u = \mathrm{e}^{-2\mathrm{i}t} \sin x \sin y. \tag{4.2}$$

We consider triangular meshes obtained by splitting the rectangle $\Omega = [0, \pi]^2$ into a total of $2m^2$ triangles, giving uniform element sizes of $h = \frac{\pi}{2^m}$. We use four different meshes, $m = 2, 3, 4, 5$. The mesh with $m = 5$ is shown in Figure 1(a). We solve (4.1) by using P^1 and P^2 elements, i.e., that $k = 1$ and $k = 2$ in (2.1), respectively. The final computation time is $t = 0.5$. To demonstrate the spatial accuracy, we fix the time step as $\Delta t = 0.001$ and the computations are performed on four levels meshes with $h = \frac{2\pi}{2^k},\ k = 2, 3, 4, 5$.

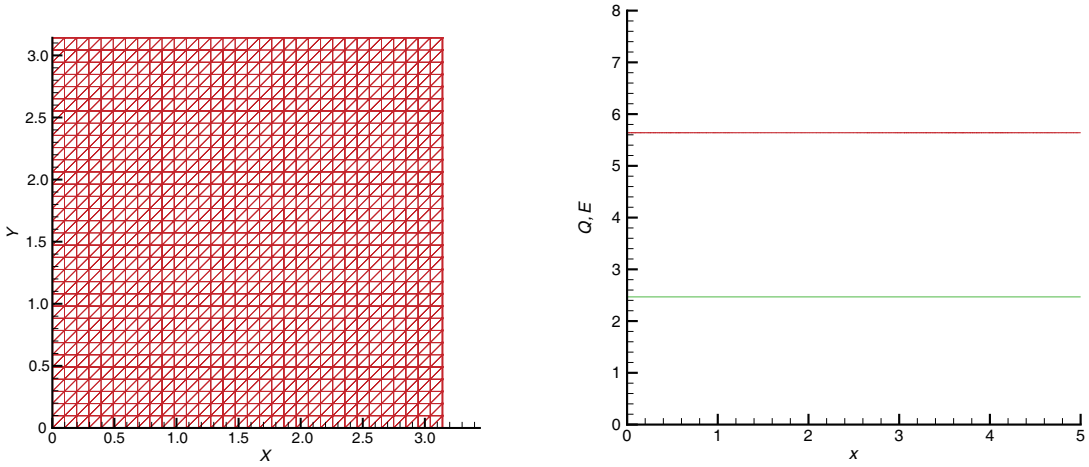

(a) The triangular mesh (b) The discretized mass and energy

Figure 1 The triangular mesh and the discretized mass and energy in Example 4.1

Table 1 The L^2, L_∞ spatial errors and order of convergence for P^1 element with $C_{11} = 0$

θ	m	L_2 error	Order	L_∞ error	Order
0.4	2	1.1328E−1	–	1.1512E−1	–
	3	3.1791E−2	1.8332	3.2590E−2	1.8206
	4	8.3377E−3	1.9309	6.4454E−3	2.3381
	5	2.1681E−3	1.9432	2.0100E−3	1.6811
0.5	2	1.0696E−1	–	7.8492E−2	–
	3	3.1179E−2	1.7784	2.3405E−2	1.7457
	4	8.4980E−3	1.8754	6.8787E−3	1.7666
	5	2.1669E−3	1.9715	1.5646E−3	2.1363
1.0	2	2.9904E−1	–	3.3903E−1	–
	3	1.4032E−1	1.0916	1.7234E−1	0.9762
	4	6.8369E−2	1.0373	8.6819E−2	0.9892
	5	3.3948E−2	1.0100	4.3638E−2	0.9924

Table 2 The L^2, L_∞ spatial errors and order of convergence for P^2 element with $C_{11} = 0$

θ	m	L_2 error	Order	L_∞ error	Order
0.4	2	1.3276E−2	–	1.3353E−2	–
	3	2.1551E−3	2.6230	1.8291E−3	2.8680
	4	4.2448E−4	2.3440	3.5120E−4	2.3808
	5	9.8766E−5	2.1036	9.2430E−5	1.9259
0.5	2	1.1453E−2	–	1.2162E−2	–
	3	1.2279E−3	3.2215	1.3451E−3	3.1766
	4	1.4700E−4	3.0623	1.6533E−4	3.0243
	5	1.7783E−5	3.0472	2.0448E−5	3.0153
1.0	2	4.0410E−2	–	4.7777E−2	–
	3	1.0085E−2	2.0025	1.2152E−2	1.9751
	4	2.5208E−3	2.0003	3.0546E−3	1.9921
	5	6.3022E−4	2.0000	7.6658E−4	1.9945

Table 3 The L^2, L_∞ spatial errors and order of convergence for P^1 element with $C_{11} = h^{-1}$

θ	m	L_2 error	Order	L_∞ error	Order
0.5	2	1.1988E−1	–	7.1699E−2	–
	3	3.7331E−2	1.6831	2.4724E−2	1.5360
	4	1.0167E−2	1.8765	6.7190E−3	1.8796
	5	2.5995E−3	1.9676	2.0355E−3	1.7229
1.0	2	1.3095E−1	–	1.0290E−1	–
	3	3.3363E−2	1.9727	2.8691E−2	1.8426
	4	9.3512E−3	1.8350	8.9633E−3	1.6785
	5	2.2164E−3	2.0769	1.9411E−3	2.2072

Table 4 The L^2, L_∞ spatial errors and order of convergence for P^2 element with $C_{11} = h^{-1}$

θ	m	L_2 error	Order	L_∞ error	Order
0.5	2	4.6918E−2	–	4.7507E−2	–
	3	4.1486E−3	3.4994	5.6162E−3	3.0805
	4	3.9769E−4	3.3829	3.8544E−4	3.8650
	5	3.1474E−5	3.6594	4.0368E−5	3.2552
1.0	2	9.0549E−3	–	8.0907E−3	–
	3	9.8008E−4	3.2077	1.0398E−3	2.9600
	4	1.0332E−4	3.2458	1.2008E−4	3.1142
	5	1.1699E−5	3.1427	1.3707E−5	3.1310

Table 5 The L^2, L_∞ temporal errors and order of convergence for IIF2 method

Δt	L_2 error	Order	L_∞ error	Order
0.2	1.2605E−2	–	1.2383E−2	–
0.1	2.5722E−3	2.2929	2.7931E−3	2.1484
0.05	6.3360E−4	2.0214	6.4481E−4	2.1149

We have proved that the LDG method (2.6)–(2.7) preserves the mass and energy conservation when the coefficient $C_{11} = 0$ in Section 2. Taking $\boldsymbol{C_{12}} = \frac{1}{2}(\theta \boldsymbol{n_1} + (1-\theta)\boldsymbol{n_2})$, $0 \leqslant \theta \leqslant 1$, we study the spatial convergence with different parameter θ. Tables 1 and 2 list the L^2 and maximum norms of the errors and orders of convergence with different values of $\theta = 0.4,\ 0.5$ and 1.0 for P^1 and P^2 element, respectively. Here, $\theta = 0.4$ corresponds to the upwind-biased flux, $\theta = 0.5$ corresponds to the central flux and $\theta = 1.0$ corresponds to the alternative flux. From Tables 1 and 2, we observe that the central fluxes achieve the optimal $(k+1)$-th order of accuracy with the stabilization parameter $C_{11} = 0$. On the other hand, the alternative flux can only achieve the suboptimal k-th order of accuracy. In fact, the alternative flux can obtain the optimal order of accuracy with the stabilization parameter C_{11} of order h^{-1} (see [6]). The errors and orders of convergence with $C_{11} = h^{-1}$ are listed in Tables 3 and 4 for P^1 and P^2 elements, respectively. We can observe that the both alternative and central flux can achieve optimal convergence with stabilization parameter of order h^{-1}.

We can conclude that the LDG methods with central flux not only preserve the mass and energy conservation but also achieve the optimal convergence. Therefore, we will select the central flux in the following numerical tests.

To estimate the rate of convergence for time, we fix the space parameter as $h = \frac{\pi}{8}$ and choose the time step as $\Delta t = 0.2\ , 0.1$ and 0.05. Table 5 shows the L^2 and maximum norms of the errors and orders of convergence for the time discretization method (3.19). These results show that the IIF2 method is indeed second-order accurate. We also check our method's ability of preserving the mass and energy conservation. The discretized expressions for conservation (1.4) and (1.5) at time $t = n\Delta t$ are written as

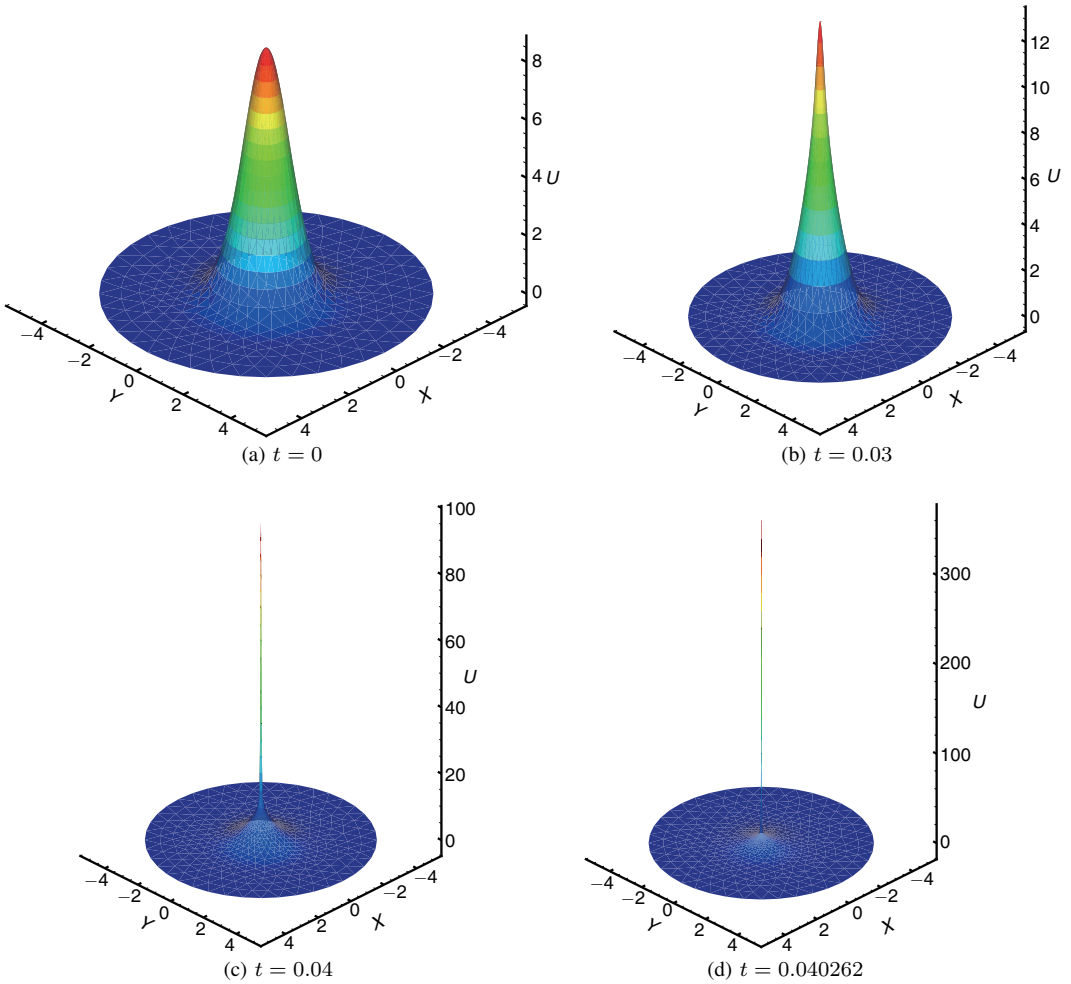

Figure 2 Images $|u|$ for the numerical solution of propagation problem in Example 4.2 at different times

$Q_n = |||u_n|||^2$, and $E_n = |||\boldsymbol{p_n}|||^2 - \frac{1}{2}|||u_n|||_4^4$, respectively. The discrete mass and energy are shown in Figure 1(b) at time $t = 5$. It shows that our proposed scheme is very robust and stable.

Furthermore, we will study the blow up properties of the solutions. Firstly, we set the initial condition with unique radially symmetric origin. Next, we take multiple points as the origin of the radially symmetric initial value to find the L^2-concentration phenomenon.

Example 4.2. In this example, we perform the computation on a circular domain $x^2 + y^2 \leqslant 5$. The initial data (1.2) is given as

$$u(x, y, 0) = 6\sqrt{2}\mathrm{e}^{-(x^2+y^2)}. \tag{4.3}$$

It has been proved in [26] that in this case, the solution is expected to blow up at the center of the domain. Therefore we refine the mesh at the center point in advance. The modulus of the solutions, $|u|$, computed by our method at times $t = 0$, $t = 0.03$, $t = 0.04$, $t = 0.040262$ are shown in Figure 2. We observe from Figure 2 that the solution blows up at the center in a finite time. This example demonstrates that our method can capture the blow up phenomenon.

Example 4.3. In this example, let us consider the following setup for the initial data:

$$u(x, y, 0) = 6\sqrt{2}(\mathrm{e}^{-((x-\sqrt{2})^2+(y-\sqrt{2})^2)} + \mathrm{e}^{-((x+\sqrt{2})^2+(y+\sqrt{2})^2)}). \tag{4.4}$$

The initial condition contains double origins of radially symmetric data. The underlying computational domain is the same as Example 4.2. The modulus of the solution computed at different times $t = 0$,

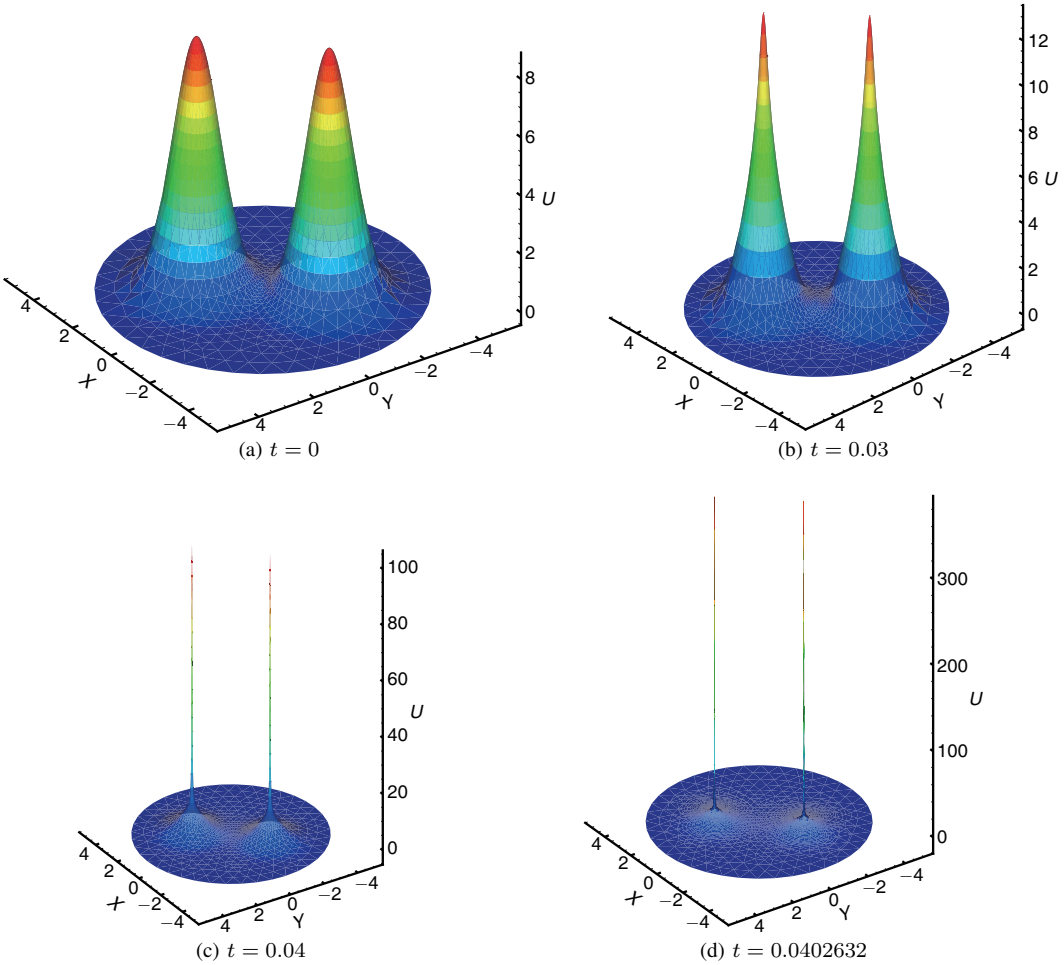

Figure 3 Images $|u|$ for the numerical solution of propagation problem in Example 4.3 at different times

$t = 0.03$, $t = 0.04$, $t = 0.040262$ are shown in Figure 3. The results seem to be in a very good agreement with the theoretical result reported in [25], which shows that the double radial origins evolve into two blow-up points where the L^2-concentration phenomenon occurs.

5 Conclusion

In this paper, we use the LDG method for solving the two-dimensional nonlinear Schrödinger (NLS) equation. The semi-discrete and fully discrete schemes obtained by the DG method are proved to preserve the mass and energy conservation when $C_{11} = 0$. These semi-discrete formulations are especially effective when they are combined with high-order, large stepsize ODE solvers for their time evolution. We introduce the Krylov IIF method in time discretization. In addition, it avoids computing the complex algebraic equation systems. This method is an efficient and attractive method for high dimensional complex partial differential equation. The obtained results confirm that our DG method is a powerful and reliable method for capturing the blow-up phenomenon.

Acknowledgements This work was supported by the Foundation of Liaoning Educational Committee (Grant No. L201604) and China Scholarship Council, National Natural Science Foundation of China (Grant Nos. 11571002, 11171281 and 11671044), the Science Foundation of China Academy of Engineering Physics (Grant No. 2015B0101021) and the Defense Industrial Technology Development Program (Grant No. B1520133015). The authors thank the referees for their valuable comments and suggestions.

References

1 Akrivis G, Dougalis V, Karakashian O. On fully discrete Galerkin methods of second-order temporal accuracy for the nonlinear Schrödinger equation. Numer Math, 1991, 59: 31–53
2 Antoine X, Bao W, Besse C. Computational methods for the dynamics of the nonlinear Schrödinger/Gross-Pitaevskii equations. Comput Phys Comm, 2013, 184: 2621–2633
3 Bao W, Jaksch D, Markowich P-A. Numerical solution of the Gross-Pitaevskii equation for Bose-Einstein condensation. J Comput Phys, 2003, 187: 318–342
4 Bassi F, Rebay S. A high-order accurate discontinuous finite element method for the numerical solution of the compressible Navier-Stokes equations. J Comput Phys, 1997, 131: 267–279
5 Bialynicki-Birula I, Mycielski J. Gaussons: Solitons of the logarithmic Schrödinger equation. Phys Scr, 1979, 20: 539–544
6 Castillo P, Cockburn B, Perugia I, et al. An a priori error analysis of the local discontinuous Galerkin method for elliptic problems. SIAM J Numer Anal, 2000, 38: 1676–1706
7 Chang Q, Jia E, Sun W. Difference schemes for solving the generalized nonlinear Schrödinger equation. J Comput Phys, 1999, 148: 397–415
8 Chen S, Zhang Y. Krylov implicit integration factor methods for spatial discretization on high dimensional unstructured meshes: Application to discontinuous Galerkin methods. J Comput Phys, 2011, 230: 4336–4352
9 Chiao R-Y, Garmire E, Townes C. Self-trapping of optical beams. Phys Rev Lett, 1964, 73: 479–482
10 Cockburn B, Shu C-W. The local discontinuous Galerkin method for time-dependent convection-diffusion systems. SIAM J Numer Anal, 1998, 35: 2440–2463
11 Cowan S, Enns R-H, Rangnekar S-S, et al. Quasi-soliton and other behaviour of the nonlinear cubic-quintic Schrödinger equation. Canad J Phys, 1986, 64: 311–315
12 Dehghan M, Taleei A. A compact split-step finite difference method for solving the nonlinear Schrödinger equations with constant and variable coefficients. Comput Phys Comm, 2010, 181: 43–51
13 Gao Z, Xie S. Fourth-order alternating direction implicit compact finite difference schemes for two-dimensional Schrödinger equations. Appl Numer Math, 2011, 61: 593–614
14 Gardner L R T, Gardner G A, Zaki S I, et al. B-spline finite element studies of the non-linear Schrödinger equation. Comput Methods Appl Mech Engrg, 1993, 108: 303–318
15 Hong J, Ji L, Liu Z. Optimal error estimates of conservative local discontinuous Galerkin method for nonlinear Schrödinger equation. ArXiv:1609.08853, 2016
16 Javidi M, Golbabai A. Numerical studies on nonlinear Schrödinger equations by spectral collocation method with preconditioning. J Math Anal Appl, 2007, 333: 1119–1127
17 Karakashian O, Akrivis G, Dougalis V. On optimal order error estimates for the nonlinear Schrödinger equation. SIAM J Numer Anal, 1993, 30: 377–400
18 Li X, Zhu J, Zhang R, et al. A combined discontinuous Galerkin method for the dipolar Bose-Einstein condensation. J Comput Phys, 2014, 275: 363–376
19 Liang X, Khaliq A, Xing Y. Fourth order exponential time differencing method with local discontinuous Galerkin approximation for coupled nonlinear Schrödinger equations. Commun Comput Phys, 2015, 17: 510–541
20 Liao H, Sun Z, Shi H. Maximum norm error analysis of explicit schemes for two-dimensional nonlinear Schrödinger equations (in Chinese). Sci Sin Math, 2010, 40: 827–842
21 Liu Y, Shu C. Analysis of the local discontinuous Galerkin method for the drift-diffusion model of semiconductor devices. Sci China Math, 2016, 59: 115–140
22 Lu W, Huang Y, Liu H. Mass preserving discontinuous Galerkin methods for Schrödinger equations. J Comput Phys, 2015, 282: 210–226
23 Lv Z-Q, Zhang L-M, Wang Y-S. A conservative Fourier pseudospectral algorithm for the nonlinear Schrödinger equation. Chin Phys B, 2014, 23: 120203
24 Meng X, Shu C, Yang Y. Superconvergence of discontinuous Galerkin methods for time-dependent partial differential equations (in Chinese). Sci Sin Math, 2015, 45: 1041–1060
25 Merle F. Construction of solutions with exactly k blow-up points for the Schrödinger equation with critical nonlinearity. Comm Math Phys, 1990, 129: 223–240
26 Merle F, Tsutsumi Y. L^2-concentration of blow-up solutions for the nonlinear Schrödinger equation with critical power nonlinearity. J Differential Equations, 1990, 84: 205–214
27 Nie Q, Zhang Y-T, Zhao R. Efficient semi-implicit schemes for stiff systems. J Comput Phys, 2006, 214: 521–537
28 Peraire J, Persson P-O. The compact discontinuous Galerkin (CDG) method for elliptic problems. SIAM J Sci Comput, 2007, 30: 1806–1824
29 Thalhammer M. High-order exponential operator splitting methods for time dependent Schrödinger equations. SIAM J Numer Anal, 2008, 46: 2022–2038
30 Tian Z, Yu P. High-order compact ADI (HOC-ADI) method for solving unsteady 2D Schrödinger equation. Comput

Phys Comm, 2010, 181: 861–868
31 Wang T, Zhao X. Optimal l^∞ error estimates of finite difference methods for the coupled Gross-Pitaevskii equations in high dimensions. Sci China Math, 2014, 57: 2189–2214
32 Wei J, Yang J. Vortex ring pinning for the gross-pitaevskii equation in three-dimensional space. SIAM J Math Anal, 2012, 44: 210–217
33 Xie S, Li G, Yi S. Compact finite difference schemes with high accuracy for one-dimensional nonlinear Schrödinger equation. Comput Methods Appl Mech Engrg, 2009, 198: 1052–1060
34 Xu Y, Shu C-W. Local discontinuous Galerkin methods for nonlinear Schrödinger equations. J Comput Phys, 2005, 205: 72–77
35 Xu Y, Shu C-W. Local discontinuous Galerkin methods for high-order time-dependent partial differential equations. Commun Comput Phys, 2010, 7: 1–46
36 Xu Y, Zhang L. Alternating direction implicit method for solving two-dimensional cubic nonlinear Schrödinger equation. Comput Phys Comm, 2012, 183: 1082–1093
37 Zhang R, Yu X, Feng T. Numerical solution of coupled nonlinear Schrödinger equation by direct discontinuous Galerkin method. Chin Phys B, 2012, 21: 030202
38 Zhang R, Yu X, Zhu J, et al. Direct discontinuous Galerkin method for nonlinear reaction-diffusion systems in pattern formation. Appl Math Model, 2014, 36: 1612–1621
39 Zhang R, Zhu J, Li X, et al. A Krylov semi-implicit DG method for the computation of ground and excited states in Bose-Einstein condensates. Appl Math Model, 2016, 40: 5096–5110
40 Zhang R, Zhu J, Yu X, et al. A conservative spectral collocation method for the nonlinear Schrödinger equation in two dimensions. Appl Math Comput, 2017, 310: 194–203